Electronic Supplementary Material (ESI) for Nanoscale Advances.

Supplementary Information

In situ Tunable Circular Dichroism of Flexible Chiral Metasurfaces Composed of Plasmonic Nanorod Trimers

Hsiang-Ting Lin[a], *Yao-Yu Hsu*[a, b], *Pi-Ju Cheng*[a], *Wei-Ting Wang*[a], *Shu-Wei Chang*[a, b], *and Min-Hsiung Shih*[a, b, c,*]

[a.] Research Center for Applied Sciences, Academia Sinica, Taipei 11529, Taiwan

[b.] Department of Photonics and Institute of Electro-Optical Engineering, National Yang Ming Chiao Tung University, Hsinchu 30010, Taiwan

[c.] Department of Photonics, National Sun Yat-sen University, Kaohsiung 80424, Taiwan

[*]E-mail: mhshih@gate.sinica.edu.tw

S1. Fabrication of the Nanorod Trimer Metasurface on PDMS Substrate

The flexible and stretchable Au nanorod trimer metasurfaces embedded in PDMS were fabricated with the bonding method as the fabrication steps shown in Fig. S1. First, the metasurface patterns were defined using electron beam lithography (EBL) on indium phosphide (InP) sacrificial substrate followed by Au deposition and lift-off process. To bond the metasurfaces on PDMS, the fabricated device was treated with 3-mercaptopropyl trimethoxysilane (MPTMS) solution to improve adhesion between Au and PDMS and then flipped upside down on the prepared PDMS mixture. After thermal curing the PDMS, the InP sacrificial substrate was removed with hydrochloric acid (HCl) solution. Due to strong covalent bond between MPTMS treated Au and PDMS, the metasurfaces were successfully transferred from InP to PDMS substrate. The SEM image of fabricated metasurfaces is shown in Fig. 1b. Since the metasurfaces were flipped upside down during the fabrication process, the trimer patterns were mirrored after PDMS bonded.

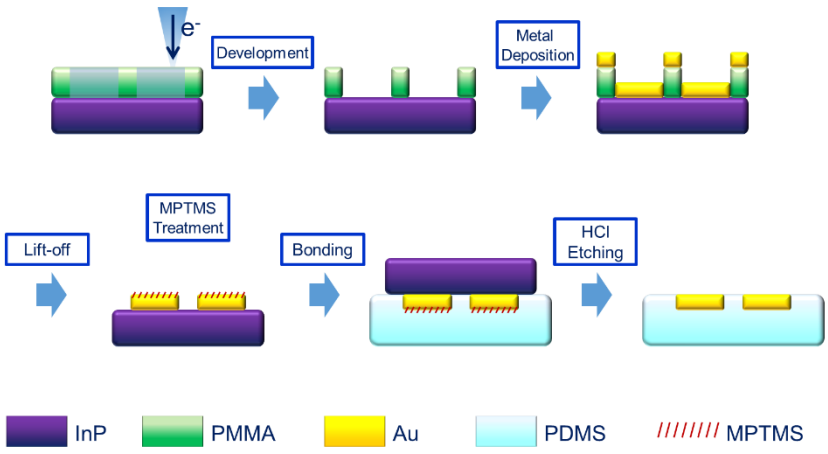

Fig. S1. Schematic illustration of the device fabrication process.

S2. Optical Characterization of the Nanorod Trimer Metasurface on PDMS Substrate

The circularly polarized extinction spectra of the fabricated chiral metasurfaces were characterized under a microscope-based transmission measurement system as shown in Fig. S2. A non-polarized white light from a tungsten–halogen source was backside-focused on the metasurfaces by a 20× objective lens, and the output signal was collected by a 10× objective lens. The polarized information of the chiral metasurface were analyzed with a broad-band quarter-wave plate) and a linear polarizer combination on the light path, and the circularly polarized spectra were recorded with a fiber connected spectrometer.

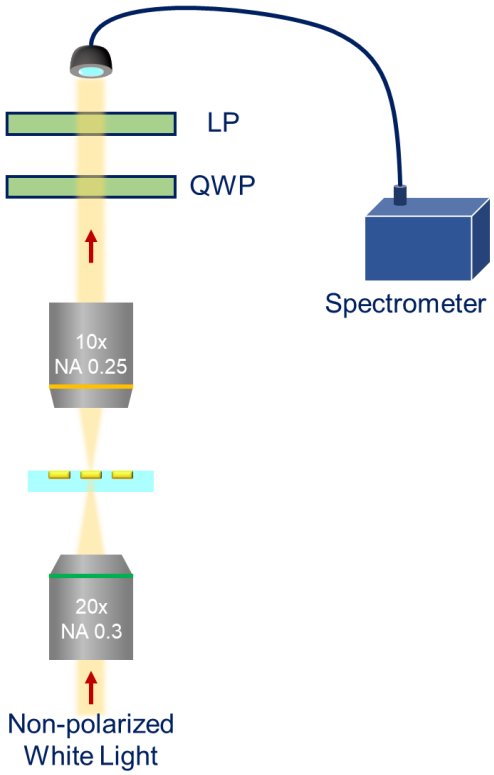

Fig. S2. Schematic illustration of the transmission measurement system.

S3. Spectral Properties of Nanorod Trimer Metasurface with Identical G_x and G_y

In order to the verify the LSPR resonances in the trimer metasurface, we compare the 3-D FDTD calculated extinction spectrum with the measured extinction spectra of the metasurface. Figure S3a presented the calculated extinction spectra of the nanorod trimer metasurfaces with $G_x = G_y = 40$ nm. Multiple extinction peaks were attributed to the LSPR coupling between different nanorod resonances. Besides, the almost overlapping extinction spectra resolved with RCP and LCP light presented in Fig. S3b indicate the achiral optical properties of the fabricated metasurfaces with $G_x \approx G_y$. A small difference in extinction spectra for LCP and RCP was attributed to the imperfection of device fabrication.

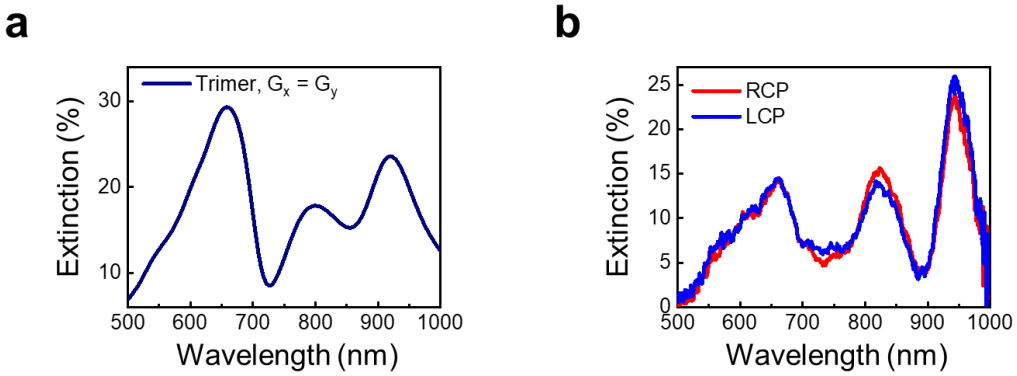

Fig. S3. (a) 3D-FDTD calculated extinction spectrum of the trimer metasurface with $G_x = G_y =$ 40 nm and (b) the measured extinction spectra of the trimer metasurface with $G_x \approx G_y$.

S4. Spectral Properties of Asymmetric Nanorod Trimer Metasurfaces and Corresponding Near-field Oscillation of the Nanorod Trimer Structure

The FDTD simulated extinction spectra of the asymmetric nanorod trimer metasurfaces with $G_x < G_y$ (G_x = 40 nm, G_y = 60 nm) and $G_x > G_y$ (G_x = 60 nm, G_y = 40 nm) under RCP and LCP incidences were displayed in Fig. S4a and S4b. The LSPR coupling between nanorods induced multiple extinction peaks can be observed in both simulated and measured spectra. Besides, the extinction peaks at around 850 nm exhibit the opposite preference to RCP and LCP light between $G_x < G_y$ and $G_x > G_y$ trimer also confirmed their optical chirality.

To understand the evolution of the chiral resonant mode of the asymmetric nanorod trimer metasurfaces, the corresponding real-time near-field oscillation of the $G_x < G_y$ trimer was presented in Supplementary movie S1 and Fig. S4c. The fields are solved under RCP incidence at wavelength of 845 nm with the 3D finite-element methods with the solutions obtained under the time-harmonic condition and displayed for 2 temporal periods. The arrows in each clip indicate the directions and magnitudes of instantaneous vectors of electric field on the exit plane (just above the nanorods). We also recorded the mode profiles in the nanorods (in the middle plane along z axis). The strong confinement of localized plasmonic modes around D_+-like dimer structures suggests that the chirality in the far-field regime. In this asymmetric trimer, the inequivalent responses around D_- or D_+ -like structures correspond to the selected absorption or reformation of waves with certain circular polarization in the far field.

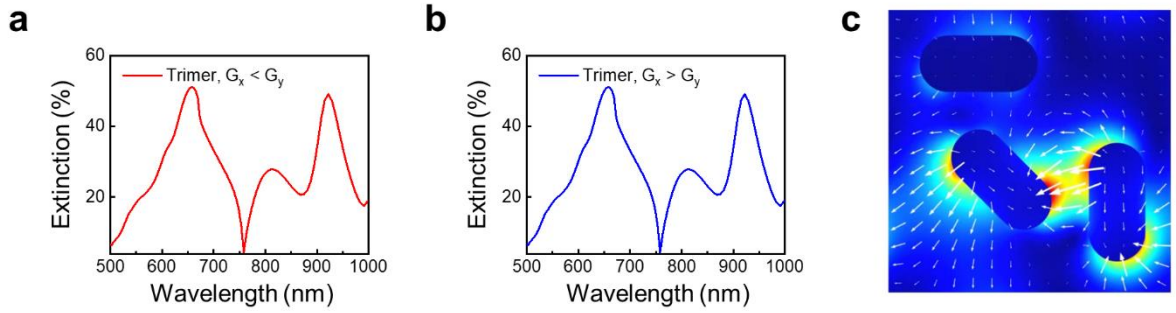

Fig. S4. 3D-FDTD calculated extinction spectra of the (a) $G_x < G_y$ (G_x = 40 nm, G_y = 60 nm) and (b) $G_x > G_y$ (G_x = 60 nm, G_y = 40 nm) asymmetric nanorod trimer metasurface. (c) One frame of the near-field oscillation of the nanorod trimer structure. The full video is provided in Supplementary movie S1.

S5. Repeatability Test of the Fabricated Flexible Chiral Metasurfaces

Durability is another figure of merits when assessing the potential of flexible devices for practical applications. We further examined the durability and repeatability of our devices by repeating multiple stretching and releasing cycles as the schematic shown in Figure S5a. The corresponding dip CD_{EXT} variation during 10^4 test cycles were presented in Figure S5b and S5c. We observed the CD_{EXT} are able to remain as ~0% at released state and ~-20% at stretched state of the flexible chiral metasurface during the repeatability test. Overall, the results reveal the high durability and repeatability of our chiral metasurface as well as its excellent tunability of CD.

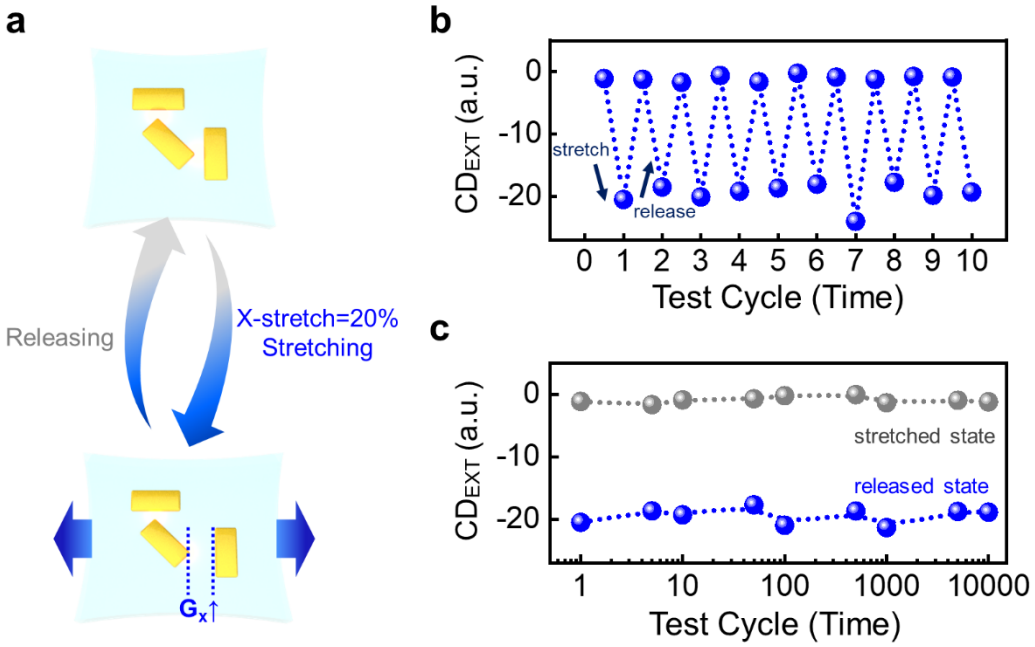

Fig. S5. (a)The repeatability test demonstration schematic of the flexible chiral metasurface. (b)The dip CD_{EXT} variations of the flexible trimer metasurfaces during first 10 test cycles. (c)The dip CD_{EXT} variations at stretched and released state of the flexible trimer metasurfaces during total 10^4 test cycles.